Sediment Organic Matter Mineralization pathways in Three Contrasted Boreal Lakes

François Clayer[1,3*], Yves Gélinas[2,3], André Tessier[1] & Charles Gobeil[1,3]

[1]Institut National de la Recherche Scientifique, Centre Eau Terre Environnement (INRS-ETE)
[2]Department of Chemistry and Biochemistry, Concordia University
[3]Geotop
[*]Corresponding author: francois.clayer@ete.inrs.ca

INTRODUCTION

The precise modelling of organic matter (OM) degradation is key in unravelling the carbon cycle and constraining methane (CH_4) and dissolved inorganic carbon (DIC) formation within sediments[1]. Despite the diversity of organic substrates (e.g. **Table 1**), the simple model molecule 'CH_2O' is often used in diagenetic modelling to represent OM[1]. Organic compounds naturally present in sediment porewater have disparate carbon oxidation state (COS in **Table 1**) which influences the amount of CH_4 and DIC produced during fermentation (e.g. **Table 1**). Hence, the model molecule used in diagenetic modelling to represent OM should be carefully assessed.

Compounds	Formula	COS	CH_4/DIC production ratio during fermentation
Glycolic acid [2]	$C_2H_4O_3$	+1.00	0.6
Glucose	$C_6H_{12}O_6$	**0.00**	**1.00**
'Fulvic acid' [2]	$C_{27}H_{28}O_7$	–0.52	1.29
C_{16}-fatty acid [1]	$C_{16}H_{32}O_2$	–1.75	2.56

Table 1: Influence of the carbon oxidation state (COS) on fermentation products

Given that reactions of sediment OM degradation (**Table 2**), in particular methanogenesis and methanotrophy, influence the carbon isotopic signature ($\delta^{13}C$) of CH_4 and DIC (**Fig. 1**), we propose to **use the $\delta^{13}C$ profiles, combined with inverse modelling, as a tool** to:

1) Unravel sediment OM mineralization pathways

2) Test the robustness of the commonly-used model-molecule 'CH_2O'

in three boreal lakes with **contrasted O_2 dynamics**.

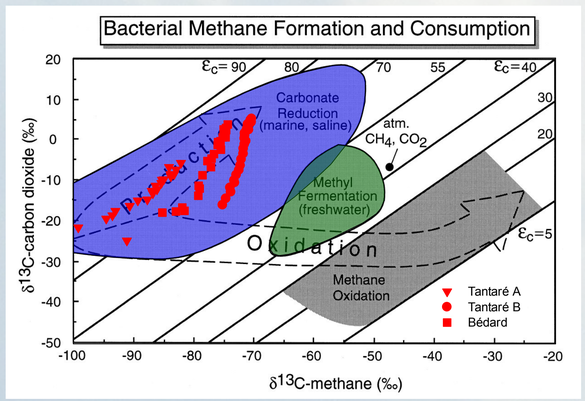

Figure 1: Combination plot of $\delta^{13}C$ of CH_4 and CO_2 [3]

MATERIALS & METHODS

CH_4 and **DIC** porewater concentrations were obtained by ***in situ*** **dialysis** (**Fig. 2C**) in triplicates:

L. Tantaré A (**oxic**) in Oct. 2015
L. Tantaré B (**seasonnally anoxic**) in Oct 2014
L. Bédard (**anoxic**) in Oct 2015

The **$\delta^{13}C$** of **CH_4** and **DIC** was determined on a gas-chromatograph coupled to an isotope-ratio mass-spectrometer (GC-C-IRMS) at Concordia University.

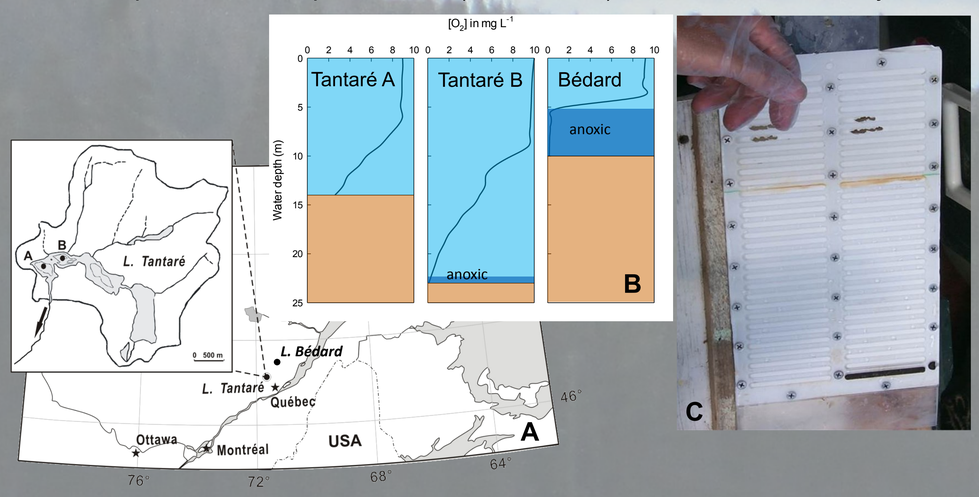

Figure 2: **A** - Location map, **B** - O_2 concentration profiles in each lake and **C** - Picture of a dialyser.

Inverse modelling of concentration profiles (Berg et al., 1998)

Assuming **steady-state** conditions and neglecting advection and bioturbation, the diagenetic equation is:

$$\frac{\partial}{\partial x}\left(\varphi D_S \frac{\partial C}{\partial x}\right) + \varphi\alpha(C_E - C) + R_{net} = 0$$

(Diffusion; Bioirrigation; Net reaction rate)

where C and C_E are the concentrations in the porewater and the bottom water, respectively, x is the depth, φ is the porosity, D_S is the diffusivity, α is the bioirrigation coefficient, and R_{net} the net reaction rate.

Equation 1

Eq. 1 is resolved via a numerical procedure to:

Constrain the **depth-intervals** where solutes are produced or consumed

Obtain the **net reaction rate (R_{net})** in each zone (**red lines** in **Fig. 4**)

Modelling $\delta^{13}C$ profiles (from Alperin et al., 1988)

The diagenesis equation for the solute containing the heavy isotop is:

$$\frac{\partial}{\partial x}\left(\varphi D_S \frac{\partial C^*}{\partial x}\right) + \varphi\alpha(C_E^* - C^*) + R^* = 0$$

Equation 2

where C^*, C_E^* and R^* are the porewater concentration, the bottom water concentration and the net reaction rate of the solute containing the heavy isotope, respectively.

and the fractionation factor α is given by:

$$\alpha = \frac{R/C}{R^*/C^*}$$ **Equation 3**

Combining **Eq. 2** and **3** we obtain:

$$\frac{\partial}{\partial x}\left(\varphi D_S \frac{\partial C^*}{\partial x}\right) + \varphi\alpha(C_E^* - C^*) + \frac{RC_r^*}{\alpha C_r} = 0$$

Measured $\delta^{13}C$ — Inverse modelling — Literature [6]

where the index "r" is for reacting species

Equation 4: Model for the estimation of $\delta^{13}C$

Eq. 4 is resolved via a MATLAB® function to obtain a modelled $\delta^{13}C$ profile (**blue** & **green lines** in **Fig. 5**).

RESULTS & DISCUSSION

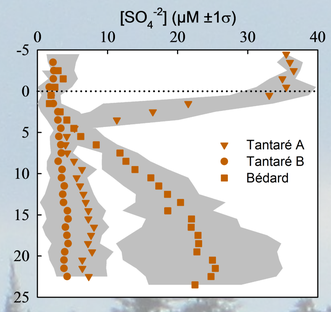

Figure 3: Sulfate concentration profiles

Reactions	Equation	Reaction rate
OM fermentation	$C_xH_yO_z + (x+\nu-z)H_2O \rightarrow 1/2(x-\nu)CH_3COOH + \nu CO_2 + (y/2-z+2\nu)H_2$	R^{OMf}
Acetoclasty	$CH_3COOH \rightarrow CH_4 + CO_2$	R^{Acet}
Hydrogenotrophy	$CO_2 + 4H_2 \rightarrow CH_4 + 2H_2O$	R^{Hydro}
Methanotrophy	$CH_4 + Oxidant \rightarrow CO_2 + Reducer$	R^{Mt}
OM oxidation	$CH_2O + Oxidant \rightarrow CO_2 + Reducer$	R^{OMx}
Fe-S cryptic cycle	$17H_2S + 8FeOOH \rightarrow SO_4^{2-} + 8FeS_2 + 8H_2 + 12H_2O + 2H^+$	$R^{Fe\text{-}S}$

Table 2: Reactions considered during sediment OM degradation

From **Table 2**, we can write: $R_{net}^{CH_4} = R^{Acet} + R^{Hydro} - R^{Mt}$ and $R_{net}^{DIC} = R^{OMf} + R^{Acet} - R^{Hydro} + R^{Mt} + R^{OMx}$

These equations along with the values of $R_{net}^{CH_4}$ and R_{net}^{DIC} in each zone are used to constrain all the possible rate values for each reaction in each zone. For example, in the deepest zone (**Fig. 4**), CH_4 is produced at about the same rate than DIC is consumed suggesting that the only reaction active in that zone is hydrogenotrophy.

Several scenarios for each lake are then defined and the best scenario is selected by fitting the simulated $\delta^{13}C$ profiles with those measured (**Fig. 5**).

This modelling approach reveals that:

- ~100 % of methanogenesis is **hydrogenotrophic** in the three lakes
- Hydrogenotrophy occurs in the shallow sediment and possibly above the sediment surface (anoxic lakes)
- The commonly-used model molecule 'CH_2O' cannot rationalize our observations in the main zone of methanogenesis:
  - Tantaré A (oxic): $R_{net}^{CH_4} < R_{net}^{DIC}$ ⇒ OM with COS > 0
  - Tantaré B (anoxic): $R_{net}^{CH_4} > R_{net}^{DIC}$ ⇒ OM with COS < 0
  - Bédard (anoxic): ⚠
- CH_4 is also produced in the deepest zone but DIC is consumed at equivalent or greater rates suggesting that H_2 doesn't come from OM fermentation but from a Fe-S cryptic cycle (see $[SO_4]$ in **Fig. 3**)
- The flux of CH_4 out of the sediments is 52, 460 and 400 in Lakes Tantaré A, Tantaré B and Bédard, respectively

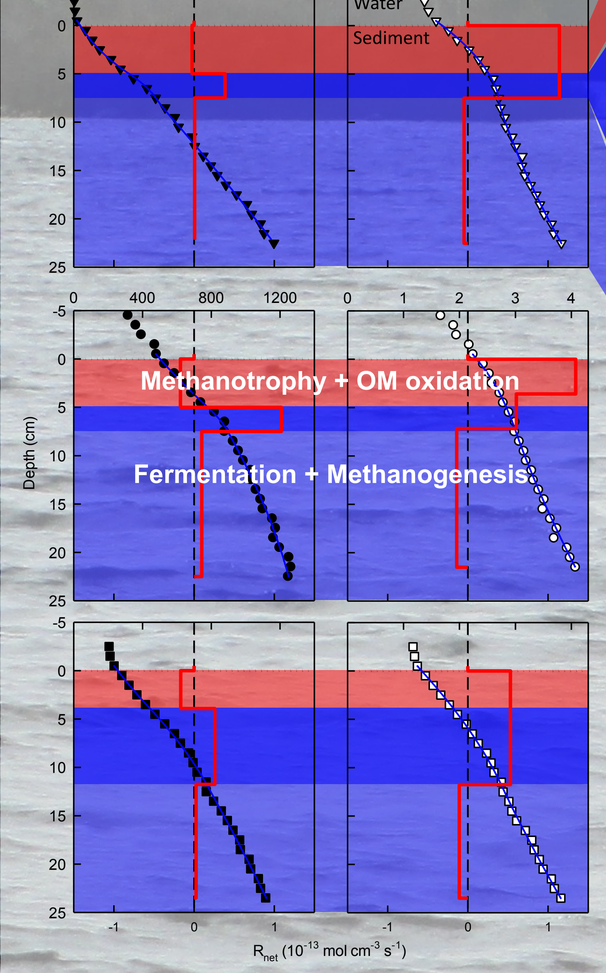

Figure 4: Measured (**symbols**) and modelled (**blue line**) concentration profiles and **R_{net}** profiles (**red line**) of CH_4 and DIC.

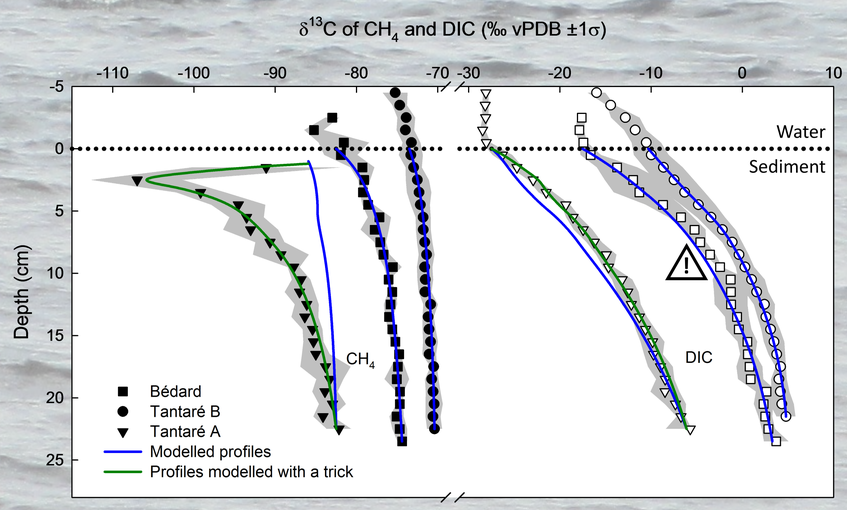

Figure 5: Measured (**symbols**) and modelled (**blue line**) $\delta^{13}C$ profiles of CH_4 and DIC. Note that the green profiles are simulated with a trick (*Ask the presenter for details).

CONCLUSIONS

The modelling of $\delta^{13}C$ profiles of CH_4 and DIC (**Fig. 5**) using a steady-state reactive-transport equation (**Eq. 4**) and the **R_{net}** values estimated by inverse modelling (**Fig. 4**) allowed us to:

- **quantify** each diagenetic pathway in L. Tantaré A and B:

Lake	CH_4 production	CH_4 consumption	DIC production due to OM	
			fermentation	oxidation
	rates in fmol C cm^{-2} s^{-1}			
Tantaré A	146	95	285	560
Tantaré B	523	185	> 128	< 540

Table 3: Rates of diagenetic pathways in L. Tantaré A & B.

Note: we were not able to conclude on diagenetic pathways in L. Bédard because simulated $\delta^{13}C$ profiles did not properly fit those measured (**Fig. 5**).

Work in progress...

- **demonstrate** that the model molecule CH_2O is not accurate to represent OM mineralized. The molecules $C_{15}H_{16}O_{22}$ (COS = +1.87) and $C_{16}H_{32}O_4$ (COS = –1.50) would be more accurate for L. Tantaré A and B, respectively.

Lastly, this work suggests that, despite anoxia, OM in L. Bédard is less reduced than that in L. Tantaré B.

ACKNOWLEDGEMENTS & REFERENCES

Fonds de recherche Nature et technologies Québec — CRSNG NSERC

Permission to work in the Tantaré Ecological Reserve from the ***Ministère du Développement Durable, de l'Environnement et de la Lutte contre les Changements Climatiques*** is gratefully acknowledged.

[1]Arning, E. T., van Berk, W. & Schulz, H.-M. (2016) Marine Chemistry 178, 8–21.
[2]Larowe, D. E. & Van Cappellen, P. (2011) Geochimica et Cosmochimica Acta 75, 2030–2042.
[3]Whiticar, M. J. (1999) Chemical Geology 161, 291-314.
[4]Berg, P., Risgaard-Petersen, N. & Rysgaard, S. (1998) Limnology and Oceanography 43, 1500-1510.
[5]Alperin, M. J., Reeburgh, W. S. & Whiticar, M. J. (1988) Global Biogeochemical Cycles 2(3), 279-288.
[6]Conrad, R., Claus, P., Chidthaisong, A., Lu, Y., Fernandez Scavino, A., Liu, Y., Angel, R., Galand, P. E., Casper, P., Guerin, F. & Enrich-Prast, A. (2014) Organic Geochemistry 73, 1-7.